




## Article

# Surface Characteristics and Microbiological Analysis of a Vat-Photopolymerization Additive-Manufacturing Dental Resin

Ericles Otávio Santos <sup>1</sup>, Pedro Lima Emmerich Oliveira <sup>2</sup>, Thaís Pereira de Mello <sup>3</sup>,  
André Luis Souza dos Santos <sup>3</sup>, Carlos Nelson Elias <sup>4</sup>, Sung-Hwan Choi <sup>5,\*</sup>  
and Amanda Cunha Regal de Castro <sup>1,\*</sup>

<sup>1</sup> Department of Pediatric Dentistry and Orthodontics, School of Dentistry, Federal University of Rio de Janeiro, Rio de Janeiro 21941617, RJ, Brazil; dr.ericlesotavio@gmail.com

<sup>2</sup> Department of Pediatric Dentistry and Orthodontics, School of Dentistry, Escola Superior São Francisco de Assis, Santa Teresa 29650000, ES, Brazil; pedroemmerich@hotmail.com

<sup>3</sup> Laboratory for Advanced Studies of Emerging and Resistant Microorganisms, Department of General Microbiology, Institute of Microbiology Paulo de Góes, Federal University of Rio de Janeiro, Rio de Janeiro 21941902, RJ, Brazil; thaispdmello@gmail.com (T.P.d.M.); andre@micro.ufrj.br (A.L.S.d.S.)

<sup>4</sup> Department of Mechanical Engineering and Materials Science, Military Institute of Engineering, Rio de Janeiro 22290270, RJ, Brazil; carloseliasime@gmail.com

<sup>5</sup> Department of Orthodontics, Institute of Craniofacial Deformity, Yonsei University College of Dentistry, Seoul 03772, Korea

\* Correspondence: selfexam@yuhs.ac (S.-H.C.); amandacunha@ortodontia.ufrj.br (A.C.R.d.C.); Tel.: +82-2-2228-3102 (S.-H.C.); +55-21-3938-2015 (A.C.R.d.C.)



**Citation:** Santos, E.O.; Oliveira, P.L.E.; de Mello, T.P.; dos Santos, A.L.S.; Elias, C.N.; Choi, S.-H.; de Castro, A.C.R. Surface Characteristics and Microbiological Analysis of a Vat-Photopolymerization Additive-Manufacturing Dental Resin. *Materials* **2022**, *15*, 425. <https://doi.org/10.3390/ma15020425>

Academic Editor:  
Filiberto Mastrangelo

Received: 25 November 2021

Accepted: 29 December 2021

Published: 6 January 2022

**Publisher's Note:** MDPI stays neutral with regard to jurisdictional claims in published maps and institutional affiliations.



**Copyright:** © 2022 by the authors. Licensee MDPI, Basel, Switzerland. This article is an open access article distributed under the terms and conditions of the Creative Commons Attribution (CC BY) license (<https://creativecommons.org/licenses/by/4.0/>).

**Abstract:** The wide application of additive manufacturing in dentistry implies the further investigation into oral micro-organism adhesion and biofilm formation on vat-photopolymerization (VP) dental resins. The surface characteristics and microbiological analysis of a VP dental resin, printed at resolutions of 50  $\mu\text{m}$  (EG-50) and 100  $\mu\text{m}$  (EG-100), were evaluated against an auto-polymerizing acrylic resin (CG). Samples were evaluated using a scanning electron microscope, a scanning white-light interferometer, and analyzed for *Candida albicans* (CA) and *Streptococcus mutans* (SM) biofilm, as well as antifungal and antimicrobial activity. EG-50 and EG-100 exhibited more irregular surfaces and statistically higher mean (Ra) and root-mean-square (rms) roughness (EG-50-Ra:  $2.96 \pm 0.32 \mu\text{m}$ ; rms:  $4.05 \pm 0.43 \mu\text{m}$ /EG-100-Ra:  $3.76 \pm 0.58 \mu\text{m}$ ; rms:  $4.79 \pm 0.74 \mu\text{m}$ ) compared to the CG (Ra:  $0.52 \pm 0.36 \mu\text{m}$ ; rms:  $0.84 \pm 0.54 \mu\text{m}$ ) ( $p < 0.05$ ). The biomass and extracellular matrix production by CA and SM and the metabolic activity of SM were significantly decreased in EG-50 and EG-100 compared to CG ( $p < 0.05$ ). CA and SM growth was inhibited by the pure unpolymerized VP resin (48 h). EG-50 and EG-100 recorded a greater irregularity, higher surface roughness, and decreased CA and SM biofilm formation over the CG.

**Keywords:** digital technologies; biomaterials; poly methyl methacrylate resin; photo-polymerizable resin; surface properties; antifungal activity; antibacterial activity

## 1. Introduction

The oral cavity is constituted of a complex and diverse microbiota that influences oral and systemic health [1], such as *Streptococcus mutans*, a major cariogenic bacterial species [2], and *Candida albicans*, a fungal species able to act as an opportunistic pathogen leading to mucosal and disseminated infections [3] under conditions that trigger the imbalance of the oral and immune system homeostasis [4–6]. Thus, the introduction of restorative or prosthetic dental materials into the oral environment might provide such an imbalance, thereby maximizing biofilm formation [7]. Recently, products manufactured with three-dimensional (3D) printing have become popular in dentistry, being increasingly used due to the ease of acquisition, processing, and manipulation of the images obtained through intraoral scanning [8,9].

The additive-manufacturing technologies: vat-photopolymerization, power bed fusion, binder jetting, material extrusion, direct energy deposition, material jetting and sheet lamination enable the application to substrates such as polymers, metals and ceramics, yielding different results regarding accuracy, precision and trueness, thus providing diverse and wide applications [10–12]. Digital-light-processing (DLP) technology is one of the first 3D-printing processes, which is categorized according to ISO/ASTM 52900/15(E) as a vat-photopolymerization (VP) process, wherein the photopolymerizable liquid is selectively cured by light projection of the object to be printed through a small projector or mirrors that display a single image at one time [13]. Each layer is photoactivated so that the resolution of the item to be printed is directly related to the number of projectors and mirrors used in the technique. That way, at each activation, solid layers of small cubic blocks, referred to as voxels, originate from the interaction of the light with the resin of origin, until the object is completely formed [10,14–17].

Dental crowns and prostheses, surgical guides and components, orthodontic aligners and appliances, as well as courseware for research and teaching, represent a reality arising from digital dentistry [10,18,19]. However, certain parameters need to be observed in order to obtain the best results from printing techniques applied in dentistry, such as the thickness of each photoactivated layer, base design, post-processing, and storage media, which are all factors that are known to influence the accuracy of 3D dental models [20]. As for printing resolutions, Shim et al. [21] and Unkovskiy et al. [22] demonstrated, through in vitro studies, that greater accuracy is obtained when objects are printed in a 90° orientation in both stereolithography (SLA) and DLP techniques. Alternatively, Hada in 2020 [23] reported that the impression in a 45° orientation presented superior accuracy in relation to 0° and 90° orientations. Shim et al. [21] also demonstrated, recently, that the printing orientation also influences the microbiological colonization capacity, as significantly lower levels of *C. albicans* were detected on objects printed in a 90° orientation rather than 45° and 0° orientations.

With respect to biocompatibility and activity against potential pathogens, photopolymers have been evaluated [24–26] regarding the antibacterial capacity of natural polymers [27] and the addition of antimicrobial agents or drugs in the synthetic polymer matrix [28–30]. Bloukh et al. [31] emphasized that the microbial-resistance phenomenon is a serious matter that threatens humanity's existence, mainly due to the indiscriminate use of antibiotic drugs. In dentistry, the development of alternative antimicrobial properties of surgical sutures [32], dental implants [33,34], restorative and denture materials [35,36] are relevant contributors to the mitigation or cessation of the use of antibiotics [37] in clinical practice.

Although there is an exponential growth in the application of additive manufacturing in dentistry, the knowledge regarding the comparison of VP dental resins to auto-polymerizing acrylic-resin systems, which are standardly applied to the manufacture of dental devices, is limited. Therefore, the present research focused on the investigation of a dental VP resin regarding surface characteristics, microbiological colonization, and antifungal/antimicrobial activities against an auto-polymerizing acrylic-resin system as the control. The null hypothesis of our study comprised: (i) the surface characteristics and biofilm formation by *C. albicans* and *S. mutans* of a VP dental resin for additive manufacturing will be similar to an auto-polymerizing acrylic resin, (ii) the 3D-printing resolution will not affect the surface characteristics and microbiological colonization of VP dental resins, and (iii) *C. albicans* and *S. mutans* growth will not be inhibited by the unpolymerized VP dental resin.

## 2. Materials and Methods

### 2.1. Materials

The sample of this study consisted of 300 specimens (4 mm in diameter × 1 mm in height) (Figure 1), divided into three groups (n = 100): control group (CG), constituted of auto-polymerizing acrylic resin, and experimental groups containing VP additive-

manufacturing dental resins printed at resolutions of 50  $\mu\text{m}$  (EG-50) and 100  $\mu\text{m}$  (EG-100) (Table 1).

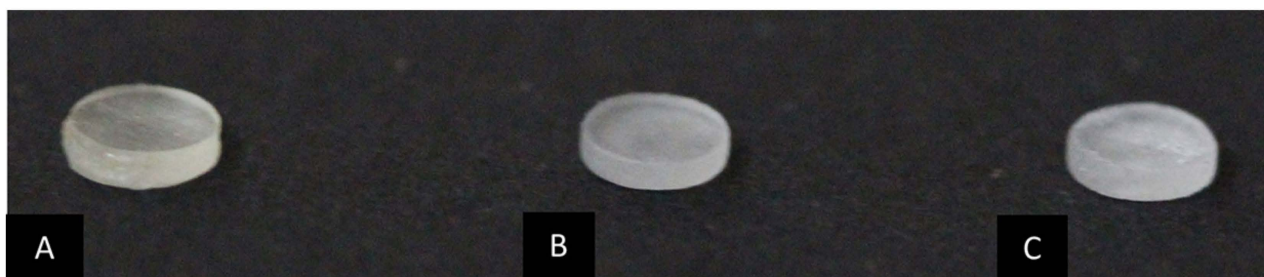


**Figure 1.** Specimen characteristics. (A): CG, auto-polymerizing acrylic resin; (B): EG-50, VP additive-manufacturing dental resin printed at 50  $\mu\text{m}$  resolution; (C): EG-100, VP additive-manufacturing dental resin printed at 100  $\mu\text{m}$  resolution.

**Table 1.** Auto-polymerizing acrylic and VP additive-manufacturing resins used in the study.

Product	Component	Manufacturer
Auto-polymerizing acrylic-resin system Ortho Class	Methyl Methacrylate Monomer, DMT, Crosslink, Methyl Ethyl Methacrylate Copolymer	Clássico São Paulo, SP, Brazil
VP additive-manufacturing dental resin COSMOS Splint	Oligomers, Monomers, Photoinitiators, Stabilizer, Pigment	Yller Pelotas, RS, Brazil

The CG was manufactured with an auto-polymerizing acrylic-resin system (Ortho-Class, São Paulo-SP, Brazil) by the same operator, with the aid of prefabricated molds of addition silicone (3 M<sup>®</sup>, São Paulo, SP, Brazil) according to the manufacturer's recommendations. To reduce the chances of air-bubble occurrence, the specimens were fabricated by an incremental-build-up technique and immersed in a pan with negative pressure (Proténi, Araraquara, SP, Brazil) during the polymerization phase. Then, the finishing of the specimens was performed sequentially using 400, 600, and 1200 g sandpapers in a Politriz metallographic machine (APL4, Arotec, Cotia, SP, Brazil) at a speed of 300 rpm/60 s for each sandpaper per specimen [38].

In the experimental groups, EG-50 and EG-100, the specimens were designed using open-source CAD software (Meshmixer v. 3.5, Autodesk, Inc., San Rafael, CA, USA) (Figure 2) with a 90° print orientation. 3D specimens were manufactured in a dental resin for additive manufacturing (Cosmos Splint, Yller, Pelotas, RS, Brazil) in a 3D printer (PHOTON S, Anycubic 3D Printing, Shenzhen, Guangdong) using digital-light-processing technology (DLP/LCD) with printing resolutions of 50 and 100  $\mu\text{m}$ . The residual surface monomers on the 3D-printed specimens were cleaned using a wipe and isopropyl alcohol. Postpolymerization was performed in accordance with the manufacturer's instructions using a UV-light polymerization unit (CureDen; DENTIS). The support structures were removed using low-speed rotary instruments (Beltec, Araraquara, SP, Brazil).

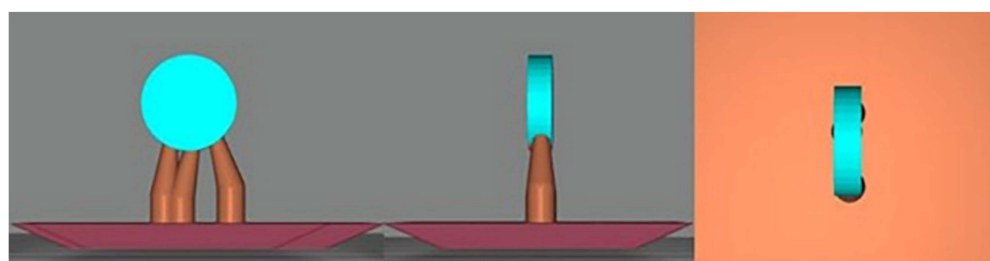


**Figure 2.** CAD design of the VP additive-manufacturing dental resin sample with 90° printing orientation (Meshmixer v. 3.5, Autodesk, Inc., CA, USA).

## 2.2. Analysis of Surface Characteristics

For the purpose of surface characterization, samples from each group were coated with gold particles and analyzed using a scanning electron microscope (Quanta FEG 250, FEI, Eindhoven, The Netherlands) at  $\times 250$ ,  $\times 500$  and  $\times 1000$  magnifications.

Morphology and surface roughness were evaluated in three samples per group, in duplicate, using a non-contact, three-dimensional, scanning white-light interferometer Zygo NewView 7100 (Zygo, Middlefield, CA, USA) using  $\times 20$  magnification lenses. The mean roughness (Ra), root mean square (rms), and mean roughness of the 3rd peak and valley (R3z) were used, with an area of  $40 \mu\text{m} \times 40 \mu\text{m}$ . The mean roughness (Ra) was quantified from the arithmetic mean of the absolute values and the ordinate distance of the points of the roughness profile in relation to the mean line within the measurement area. The root-mean-square (rms) deviation was defined as the square root of the mean of the ordinates' squares of the effective profile in relation to the mean line within the measurement path. Finally, the mean roughness of the 3rd peak and valley (R3z) was obtained by the arithmetic mean of the partial roughness values corresponding to each of the five modules.

## 2.3. Microbiological Analysis

Prior to the beginning of microbiological analysis, the specimens were sterilized by ultraviolet (UV) light for 30 min [39] and then allocated to cell-culture microplates with 96 wells each (Kasvi<sup>®</sup>, São José dos Pinhais, Paraná, Brazil) wherein  $1 \times 10^6$  *Candida albicans* yeasts and  $1 \times 10^6$  colony-forming units (CFUs) of *Streptococcus mutans* were added. The systems were kept in an oven (Quimis<sup>®</sup>, Diadema, Brazil) at a controlled temperature of  $37 \text{ }^\circ\text{C} \pm 1 \text{ }^\circ\text{C}$  for 24, 48, and 72 h, in brain heart infusion (BHI). After each of the different timepoints, the resins were re-allocated into new 96-well plates, and the biomass, extracellular matrix, and metabolic activity were quantified in triplicate.

The biomass formed by different micro-organisms was evaluated according to the method described by Peeters (2008) [40]. The culture media were discarded and the biomass was fixed with 100% methanol (200  $\mu\text{L}$ ) for 15 min. The systems were dried at room temperature for 5 min and then a solution containing 0.4% crystal violet (200  $\mu\text{L}$ ) was added, and the plates were incubated for 20 min. To remove excess dye, the systems were washed again with PBS. Subsequently, the biomass was decolorized with 30% acetic acid (200  $\mu\text{L}$ ) for 5 min. The bleach solution (100  $\mu\text{L}$ ) was transferred to another 96-well plate, and the absorbance was measured at 590 nm using a SpectraMax M3 microplate reader (Molecular Devices, San Jose, CA, USA).

The extracellular matrix was quantified according to the method described by Choi in 2015 [41]. The culture medium was discarded and a solution containing 0.1% safranin (200  $\mu\text{L}$ ) at room temperature was added to the wells for 5 min. To remove excess dye, the system was washed with PBS. Subsequently, the extracellular matrix was decolorized with 30% acetic acid (200  $\mu\text{L}$ ) for 5 min. The bleach solution (100  $\mu\text{L}$ ) was transferred to another 96-well plate, and the absorbance was measured at 530 nm using a SpectraMax M3 microplate reader.

The metabolic activity of the microbial biomass formed after each incubation time was evaluated by reducing XTT (2,3-bis(2-methoxy-4-nitro-5-sulfophenyl)-5-[(phenylamino)carbonyl]-2H-tetrazolium hydroxide (XTT; Sigma-Aldrich, Saint Louis, MO, USA). A solution of XTT at a final concentration of 200  $\mu\text{g}/\text{mL}$  and 0.04 mM of menadione was added to the wells for 4 h in the absence of light. After this time, the color change was measured using a SpectraMax M3 microplate reader at a wavelength of 492 nm [36].

## 2.4. Antifungal and Antimicrobial Activity Testing

The antifungal and antimicrobial activities of unpolymerized VP resin were evaluated at concentrations of 100%, 90%, 80%, 70%, 60%, 50%, 40%, 30%, 20%, 10%, and 0%, diluted in BHI medium according to modified versions of the CLSI M27-A3 and CLSI M07-A9 (2012) for yeasts and bacteria, respectively. To each of the wells (96-well plate),  $1 \times 10^3$  yeasts of *C.*

*albicans* and  $1 \times 10^4$  CFU of *S. mutans* were added. The following controls were performed: (i) pure BHI medium, (ii) pure unpolymerized VP resin, and (iii) BHI medium with microorganisms. The plates were visually read after incubation at 37 °C for 48 h [42,43].

### 2.5. Statistical Analysis

The statistical analysis was performed using the Statistical Package for Social Science IBM SPSS software for Windows (version 20.0, SPSS Inc., Chicago, IL, USA). The adherence to the normal curve was assessed with the Shapiro–Wilk test. After verifying the normal distribution, the control- and experimental-group comparisons of surface roughness and microbiological data were performed using the one-way analysis of variance (ANOVA) followed by Tukey’s and Dunnett’s multiple-comparisons tests, respectively. In all of the analyses, the significance level was set at 5%.

## 3. Results

### 3.1. Surface Characteristics

#### 3.1.1. Scanning Electron Microscope (SEM)

SEM images of the auto-polymerizing acrylic and VP resin samples are illustrated in Figure 3. According to the analysis of the images, a flat but grooved surface was observed in the CG, with clear notches resulting from the polishing sandpapers. A distinguishable, corrugated and more irregular surface was noticed in the experimental groups (EG-50 and EG-100), which might be attributed to the photopolymers’ layer-deposition process (Figure 3).

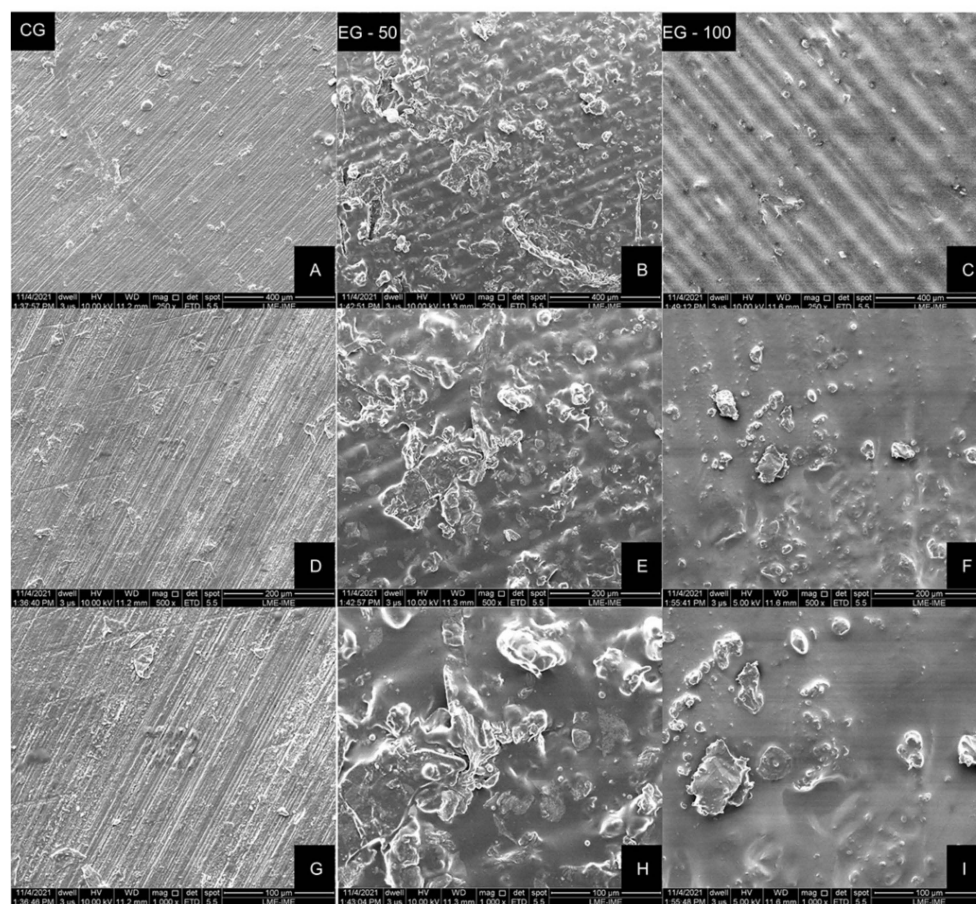


**Figure 3.** Representative SEM images of specimens from each group. (A, D and G), CG—auto-polymerizing acrylic resin. (B, E and H)—EG-50, VP dental resin printed with 50 μm resolution. (C, F and I)—EG-100, VP dental resin printed with 100 μm resolution. Magnifications: (A–C),  $\times 250$ ; (D–F),  $\times 500$ ; (G–I),  $\times 1000$ .

### 3.1.2. Surface Roughness

The surface-roughness data are presented in Table 2. Intergroup comparisons indicated a statistically significant difference in all of the roughness parameters evaluated ( $p < 0.05$ ). The experimental groups, EG-50 (Ra:  $2.96 \pm 0.32 \mu\text{m}$ ; rms:  $4.05 \pm 0.43 \mu\text{m}$ ) and EG-100 (Ra:  $3.76 \pm 0.58 \mu\text{m}$ ; rms:  $4.79 \pm 0.74 \mu\text{m}$ ), recorded the highest mean roughness and root mean square, compared to the control group (Ra:  $0.52 \pm 0.36 \mu\text{m}$ ; rms:  $0.84 \pm 0.54 \mu\text{m}$ ). As for R3z, a statistically significant difference was observed only in EG-100 compared to CG (EG-100:  $58,324.17 \pm 4936.48 \text{ nm}$ ; CG:  $31,022.08 \pm 16,470.44 \text{ nm}$ ) (Table 2). Images of the three-dimensional morphology of the samples from each group are shown in Figure 4.

**Table 2.** Descriptive statistics (mean and standard deviation) of the surface roughness analysis.

Groups	Ra ( $\mu\text{m}$ )	$p$ -Value	rms ( $\mu\text{m}$ )	$p$ -Value	R3z (nm)	$p$ -Value
CG	$0.52 \pm 0.36 a$		$0.84 \pm 0.54 a$		$31,022.08 \pm 16,470.44 a$	
EG-50	$2.96 \pm 0.32 b$	<0.001	$4.05 \pm 0.43 b$	<0.001	$53,966.22 \pm 6866.32 ab$	0.042
EG-100	$3.76 \pm 0.58 b$		$4.79 \pm 0.74 b$		$58,324.17 \pm 4936.48 b$	

Ra, mean roughness; rms, root mean square; R3z, mean roughness of the 3rd peak and valley. CG, acrylic-resin group; EG-50, VP resin printed with  $50 \mu\text{m}$  resolution; EG-100, VP resin printed with  $100 \mu\text{m}$  resolution. Distinct letters indicate statistically significant difference with ANOVA/Tukey test ( $\alpha = 0.05$ ).

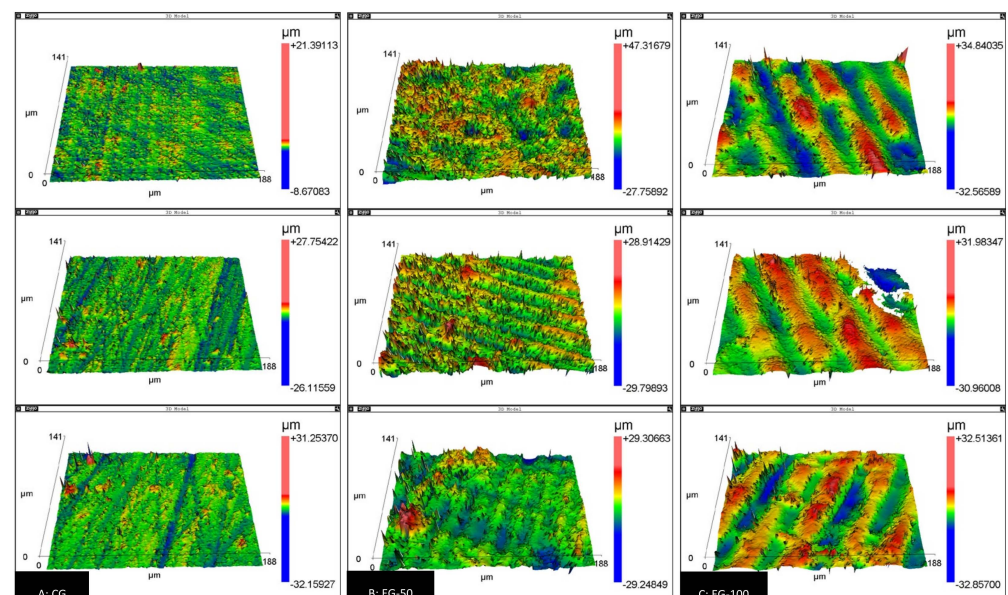


**Figure 4.** Three-dimensional surface-morphology images obtained with a scanning white-light interferometer (scan area:  $40 \mu\text{m}^2$ ) (A): CG, auto-polymerizing acrylic resin; (B): EG-50, VP resin printed with  $50 \mu\text{m}$  resolution; (C): EG-100, VP resin printed with  $100 \mu\text{m}$  resolution.

### 3.2. Quantification and Kinetics of Biofilm Formation

The biomass, metabolic-activity, and extracellular-matrix data of the micro-organisms *C. albicans* and *S. mutans* that were evaluated in the different study groups are presented in Figures 5–7, respectively.

A significantly higher quantification of the biomass of *C. albicans* was observed in CG in relation to EG-100 at 72 h ( $p < 0.05$ ). The CG samples also presented a statistically greater quantification of the biomass of *S. mutans* compared to the experimental groups (EG-50 and EG-100) at 24 h and 72 h ( $p < 0.05$ ), and to EG-50 at 48 h ( $p < 0.05$ ) (Figure 5).

No significant differences were observed in the metabolic activity of *C. albicans* among the study groups. However, a statistically higher metabolic activity of *S. mutans* was observed in CG compared to EG-50 and EG-100 at 48 h ( $p < 0.05$ ), and in CG compared to EG-50 at 72 h ( $p < 0.05$ ) (Figure 6).

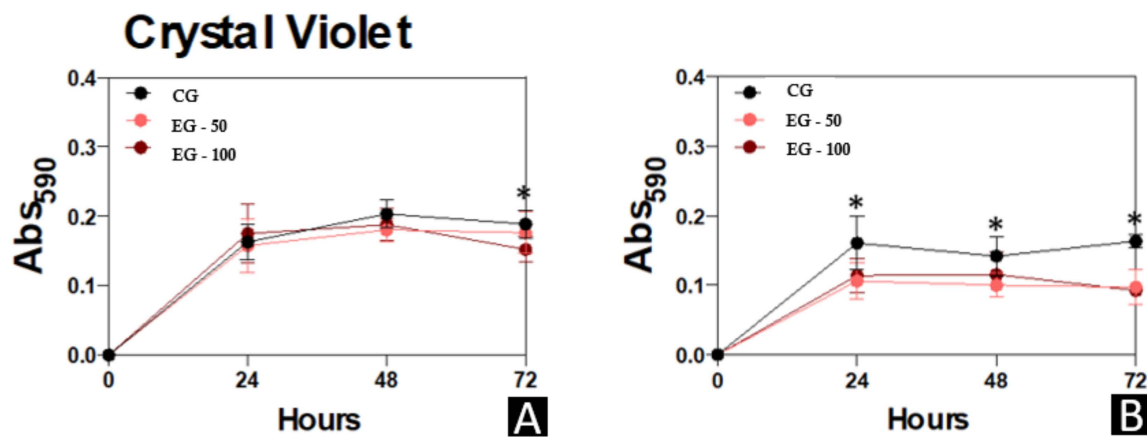


**Figure 5.** Biofilm formation by *C. albicans* and *S. mutans* for 24, 48, and 72 h at 37 °C. (A), *C. albicans*. (B), *S. mutans*. At each time point evaluated, the systems were processed to detect biomass by incorporating a crystal-violet solution at 590 nm. Results are expressed as the mean  $\pm$  standard deviation of three independent replicates. \*  $p < 0.05$ .

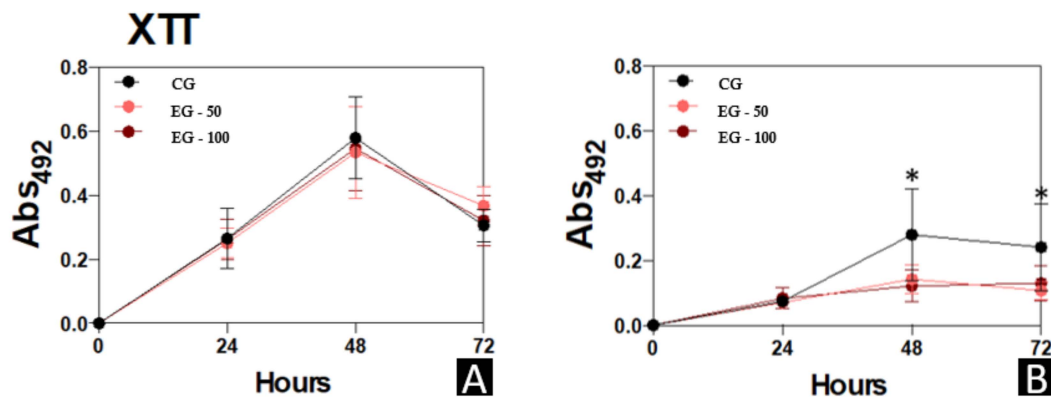


**Figure 6.** Biofilm formation by *C. albicans* and *S. mutans* for 24, 48, and 72 h at 37 °C. (A), *C. albicans*. (B), *S. mutans*. At each time point evaluated, the systems were processed to detect metabolic activity by reducing XTT in menadione by viable cells at 492 nm. Results are expressed as the mean  $\pm$  standard deviation of three independent replicates. \*  $p < 0.05$ .

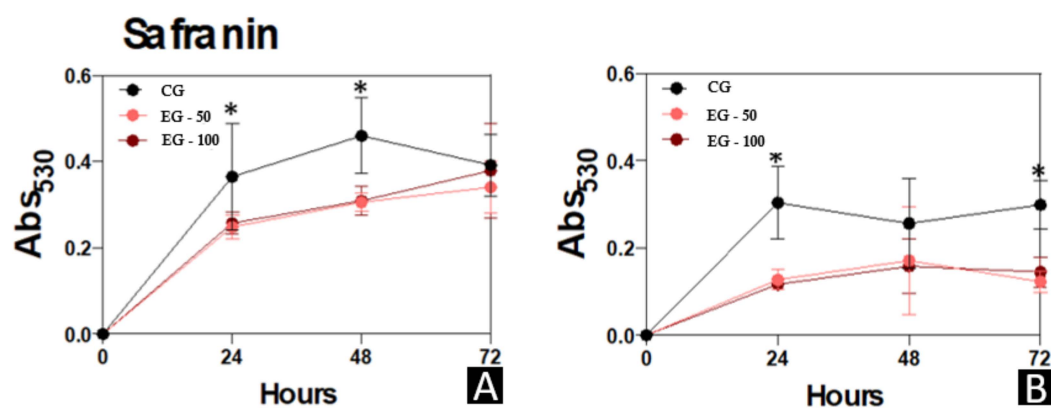


**Figure 7.** Extracellular matrix in biofilm formed by *C. albicans* and *S. mutans* for 24, 48, and 72 h at 37 °C. (A), *C. albicans*. (B), *S. mutans*. At each time point evaluated, the systems were processed to detect extracellular matrix by staining with safranin at 530 nm. Results are expressed as the mean  $\pm$  standard deviation of three independent replicates. \*  $p < 0.05$ .

CG presented a higher extracellular matrix production of biofilm formation by *C. albicans* in relation to EG-50 and EG-100 at 24 h ( $p < 0.05$ ) and 48 h ( $p < 0.01$ ). Also, the biofilm formed by *S. mutans* recorded increased records of extracellular matrix production in CG compared to EG-50 and EG-100 at 24 h ( $p < 0.001$ ) and 72 h ( $p \leq 0.001$ ) (Figure 7).

### 3.3. Antifungal and Antimicrobial Activity Testing

Antifungal and antimicrobial activity testing indicated that, with the exception of pure unpolymerized VP resin (100%), all of the VP-resin dilutions and control systems of BHI medium with micro-organisms presented *C. albicans* and *S. mutans* growth after a 48 h incubation period at 37 °C.

## 4. Discussion

The wide application of additive-manufacturing resources in dentistry implies the further investigation into the capacity of oral micro-organisms to adhere and form biofilm on vat-photopolymerization (VP)-resin substrates. This in vitro study analyzed the surface characteristics of a VP dental resin for additive manufacturing, printed at resolutions of 50 and 100  $\mu\text{m}$ , in order to determine whether there would be a difference in the surface characteristics and microbiological activity compared to an auto-polymerizing acrylic resin. This investigation directly applies to the manufacture of intraoral devices that usually remain in the oral cavity for a long period of time [4,5].

The analysis of the images obtained with SEM (Figure 3) and with the scanning white-light interferometer (Figure 4) reveals the surface grooves caused by the sequential finishing with the sandpaper strips in the CG, and the printing traces of each resin layer deposition in the EG-50 and EG-100.

When investigating the surface quality of a material-jetting additive-manufacturing process, Udriou et al. [44] observed that the platen orientation and finishing type were influential factors of the surface roughness, of which their best interaction produced roughness values (Ra) of up to 0.5  $\mu\text{m}$ . On the other hand, previous studies reported Ra values ranging from 0.87 to 5.77  $\mu\text{m}$  [45–48], which were attributed to the methodological difference of the experiments, such as diverse materials, printers, additive-manufacturing technologies, printing parameters, build orientations, and measurement techniques. In the present study, the VP resin samples recorded Ra values that were approximately six to eight times higher (EG-50: 2.9  $\mu\text{m}$  and EG-100: 3.7  $\mu\text{m}$ ) compared to the auto-polymerizing acrylic-resin samples (CG: 0.5  $\mu\text{m}$ ). Despite the fact that the surface roughness of 3D printed objects has been previously related to the thickness of each layer deposition [49,50], the Ra parameter in the present study was not significantly influenced by the layer thicknesses of 50 and 100  $\mu\text{m}$ .

The literature shows that an increased surface roughness above the Ra threshold of 0.2  $\mu\text{m}$  [51] facilitates a greater microbiological colonization [52,53] owing to features such as the greater area available for micro-organisms adhesion, the protection from shear forces and the chemical changes that favor physicochemical interactions [54]. Conversely, despite the higher average Ra values, EG-50 and EG-100 recorded a decreased *C. albicans* and *S. mutans* biofilm formation in comparison to CG. These findings may be attributed to the influence of the surface energy and the charge of the photopolymers for additive manufacturing on micro-organism colonization and growth [7,55]. Cell-surface charge is essential for modulating microbial adhesion and aggregation [56], and since Steiner et al. [57] presented their discoveries of peptides' antibacterial activity against both bacteria and eukaryotic cells, these proteins have been employed in polymeric structures. A common feature is the combination of amino acids with polar and non-polar side chains, leading to amphiphilic structures in these peptides [25].

The negative surface charge of *S. mutans* and *C. albicans*, which is attributed to the phospholipids and teichoic acids of gram-positive bacteria and the sialic acid of the *Candida* cell wall [58], is attracted by the positive surface charge of the auto-polymerizing acrylic



resin and photopolymers. However, positively, neutral and negatively charged functional groups can vary depending on the polymer's composition [25,59–61].

There is also a strong correlation between attractive hydrophobic and repulsive electrostatic forces with *C. albicans*' ability to adhere to polymeric surfaces, which are important in the initial adherence to the dental resin, providing means for further attachment and colonization [62,63]. The poly methyl methacrylate has monomer units exposed on its surface that interact with the hydrophobic domains, thus favoring the immediate adhesion of the fungi [63,64]. Secondly to hydrophobic forces, there are electrostatic interactions that favor the adhesion process of micro-organisms [65].

Another factor that may influence microbial colonization is the orientation of the object at the time of photopolymer printing. In 2020, Shim et al. [21] demonstrated that objects printed with a 90° orientation, as well as those printed in the present study, had significantly lower levels of colonization by *C. albicans* than those printed at 0° and 45°. In addition, the 90° printing orientation was chosen as it allowed for less contact with the supporting pillar of the specimen during the printing process, thereby reducing the interference on the sample's surface.

The potential of microbiological growth inhibition by the photopolymers should also be highlighted. Many authors have previously discussed the benefits of introducing components with antibacterial potential to additive manufacturing, especially against micro-organisms that have, to some degree, bacterial resistance [25,66–68]. The use of phytochemical agents has also become a prominent alternative strategy against bacteria and fungi. Moussaoui et al. [69] showed promising results of the antibacterial, antifungal and antioxidant power of *Lepidium sativum* seed oil. Meanwhile, the selection of antimicrobial components needs to be done carefully, as there is a great similarity between human cells and fungi (both eukaryotic organisms), which hampers the use of a substance that only has selective toxicity for pathogens [70].

The antifungal and antimicrobial potential of photopolymers would be crucial in dentistry with regards to the manufacturing of several intraoral devices such as prostheses and orthodontic retainers. The photopolymer evaluated in the present study inhibited the growth of *S. mutans* and *C. albicans* in its pure unpolymerized form for a period of 48 h. However, once diluted, even at the lowest concentration of BHI (90% photopolymer and 10% BHI), there was a positive microbiological growth. Therefore, further investigation is necessary to evaluate whether the inhibition of microbiological growth in the pure unpolymerized photopolymer is due to the lack of BHI medium nutrients or to a soluble component with antifungal and antimicrobial properties that loses its potential of action when in contact with the BHI medium.

## 5. Conclusions

Within the limitation of this in vitro study, the following conclusions can be drawn:

- VP dental-resin samples recorded a greater irregularity, higher surface roughness, and decreased *C. albicans* and *S. mutans* biofilm formation over the auto-polymerizing acrylic resin.
- Surface characteristics and microbiological colonization of VP resins were not significantly affected by the 3D-printing resolutions of 50 and 100 µm.
- VP dental resin inhibited *C. albicans* and *S. mutans* growth only in its pure, unpolymerized form for an incubation period of 48 h.

**Author Contributions:** Conceptualization, P.L.E.O. and A.C.R.d.C.; methodology, E.O.S., T.P.d.M., C.N.E. and A.C.R.d.C.; formal analysis, T.P.d.M. and A.C.R.d.C.; investigation, E.O.S., T.P.d.M. and A.C.R.d.C.; resources, P.L.E.O. and A.C.R.d.C.; data curation, T.P.d.M. and A.C.R.d.C.; writing—original draft preparation, E.O.S. and A.C.R.d.C.; writing—review and editing, P.L.E.O., T.P.d.M., A.L.S.d.S., C.N.E., S.-H.C. and A.C.R.d.C.; visualization, E.O.S. and A.C.R.d.C.; supervision, A.C.R.d.C.; project administration, S.-H.C. and A.C.R.d.C.; funding acquisition, S.-H.C. and A.C.R.d.C. All authors have read and agreed to the published version of the manuscript.

**Funding:** This study was financed in part by the Coordenação de Aperfeiçoamento de Pessoal de Nível Superior—Brazil (CAPES)—Finance Code 001 and was supported by the Korea Medical Device Development Fund grant funded by the Korea government (the Ministry of Science and ICT, the Ministry of Trade, Industry and Energy, the Ministry of Health & Welfare, the Ministry of Food and Drug Safety) (Project Number: KMDF\_PR\_20200901\_0067-01) and was supported by a grant from the Korea Health Technology R&D Project through the Korea Health Industry Development Institute (KHIDI), funded by the Ministry of Health & Welfare, Republic of Korea (grant number: HI20 C0611).

**Institutional Review Board Statement:** Not applicable.

**Informed Consent Statement:** Not applicable.

**Data Availability Statement:** The datasets generated and analyzed during the current study are available from the corresponding author upon reasonable request.

**Acknowledgments:** The authors would like to acknowledge the contribution of Mariana Braz Herzog in this study.

**Conflicts of Interest:** The authors declare no conflict of interest.

### Abbreviations

<b>Abs</b>	Absorbance
<b>BHI</b>	Brain Heart Infusion
<b>CA</b>	<i>Candida albicans</i>
<b>CG</b>	Control group
<b>CFU</b>	Colony forming units
<b>DLP</b>	Digital light processing technology
<b>EG-50</b>	3D resin experimental group with 50 µm resolution
<b>EG-100</b>	3D resin experimental group with 100 µm resolution
<b>µL</b>	Microliter
<b>µm</b>	Micrometer
<b>mm</b>	Millimeter
<b>nm</b>	Nanometer
<b>n</b>	Sample size
<b>rpm</b>	Rotations per minute
<b>Ra</b>	Surface roughness
<b>rms</b>	Root mean square
<b>R3z</b>	Roughness of the 3rd peak and valley
<b>SEM</b>	Scanning electron microscope
<b>SM</b>	<i>Streptococcus mutans</i>
<b>3D</b>	Three-dimensional
<b>UV</b>	Ultraviolet
<b>VP</b>	Vat photopolymerization
<b>XTT</b>	2,3-bis(2-methoxy-4-nitro-5-sulfophenyl)-5-[(phenylamino)carbonyl]-2H-tetrazolium hydroxide

### References

- Zhang, Y.; Wang, X.; Li, H.; Ni, C.; Du, Z.; Yan, F. Human oral microbiota and its modulation for oral health. *Biomed. Pharm.* **2018**, *99*, 883–893. [[CrossRef](#)]
- Lemos, J.A.; Quivey, R.G.; Koo, H.; Abranches, J. *Streptococcus mutans*: A new Gram-positive paradigm? *Microbiology* **2013**, *159*, 436–445. [[CrossRef](#)]
- Masuoka, J. Surface glycans of *Candida albicans* and other pathogenic fungi: Physiological roles, clinical uses, and experimental challenges. *Clin. Microbiol. Rev.* **2004**, *17*, 281–310. [[CrossRef](#)] [[PubMed](#)]
- Zijngel, V.; van Leeuwen, M.B.; Degener, J.E.; Abbas, F.; Thurnheer, T.; Gmur, R.; Harmsen, H.J. Oral biofilm architecture on natural teeth. *PLoS ONE* **2010**, *5*, e9321. [[CrossRef](#)]
- Rabin, N.; Zheng, Y.; Opoku-Temeng, C.; Du, Y.; Bonsu, E.; Sintim, H.O. Biofilm formation mechanisms and targets for developing antibiofilm agents. *Future Med. Chem.* **2015**, *7*, 493–512. [[CrossRef](#)]
- Marcotte, H.; Lavoie, M.C. Oral microbial ecology and the role of salivary immunoglobulin A. *Microbiol. Mol. Biol. Rev.* **1998**, *62*, 71–109. [[CrossRef](#)]

7. Hao, Y.; Huang, X.; Zhou, X.; Li, M.; Ren, B.; Peng, X.; Cheng, L. Influence of Dental Prosthesis and Restorative Materials Interface on Oral Biofilms. *Int. J. Mol. Sci.* **2018**, *19*, 3157. [[CrossRef](#)] [[PubMed](#)]
8. Kim, S.Y.; Shin, Y.S.; Jung, H.D.; Hwang, C.J.; Baik, H.S.; Cha, J.Y. Precision and trueness of dental models manufactured with different 3-dimensional printing techniques. *Am. J. Orthod. Dentofac. Orthop.* **2018**, *153*, 144–153. [[CrossRef](#)] [[PubMed](#)]
9. Camargo, I.F.; Manetti, L.P.; Zeczkowski, M.; Sundfeld Neto, D.; Pini, N.I.P.; Mori, A.A.; Ferrairo, B.M.; Lima, F.F. Sistemas cad/cam e suas aplicações na odontologia: Revisão da literatura. *REVISTA UNINGÁ* **2018**, *55*, 221–228.
10. Revilla-León, M.; Özcan, M. Additive Manufacturing Technologies Used for Processing Polymers: Current Status and Potential Application in Prosthetic Dentistry. *J. Prosthodont. Off. J. Am. Coll. Prosthodont.* **2019**, *28*, 146–158. [[CrossRef](#)]
11. Nath, S.D.; Nilufar, S. An Overview of Additive Manufacturing of Polymers and Associated Composites. *Polymers* **2020**, *12*, 2719. [[CrossRef](#)]
12. Pagac, M.; Hajnys, J.; Ma, Q.-P.; Jancar, L.; Jansa, J.; Stefek, P.; Mesicek, J. A Review of Vat Photopolymerization Technology: Materials, Applications, Challenges, and Future Trends of 3D Printing. *Polymers* **2021**, *13*, 598. [[CrossRef](#)] [[PubMed](#)]
13. ISO/ASTM 52900:2015(E). *Standard Terminology for Additive Manufacturing—General Principles—Terminology*; ASTM International: West Conshohocken, PA, USA, 2015. [[CrossRef](#)]
14. Voet, V.S.D.; Strating, T.; Schnelting, G.H.M.; Dijkstra, P.; Tietema, M.; Xu, J.; Woortman, A.J.J.; Loos, K.; Jager, J.; Folkersma, R. Biobased Acrylate Photocurable Resin Formulation for Stereolithography 3D Printing. *ACS Omega* **2018**, *3*, 1403–1408. [[CrossRef](#)] [[PubMed](#)]
15. Dawood, A.; Marti Marti, B.; Sauret-Jackson, V.; Darwood, A. 3D printing in dentistry. *Br. Dent J.* **2015**, *219*, 521–529. [[CrossRef](#)]
16. Salmoria, G.V.; Ahrens, C.H.; Beal, V.E.; Pires, A.T.N.; Soldi, V. Evaluation of post-curing and laser manufacturing parameters on the properties of SOMOS 7110 photosensitive resin used in stereolithography. *Mater. Des.* **2009**, *30*, 758–763. [[CrossRef](#)]
17. Borrello, J.; Nasser, P.; Iatridis, J.; Costa, K.D. 3D Printing a Mechanically-Tunable Acrylate Resin on a Commercial DLP-SLA Printer. *Addit. Manuf.* **2018**, *23*, 374–380. [[CrossRef](#)] [[PubMed](#)]
18. Bhargav, A.; Sanjairaj, V.; Rosa, V.; Feng, L.W.; Fuh Yh, J. Applications of additive manufacturing in dentistry: A review. *J. Biomed. Mater. Res. Part B Appl. Biomater.* **2018**, *106*, 2058–2064. [[CrossRef](#)]
19. Javaid, M.; Haleem, A. Current status and applications of additive manufacturing in dentistry: A literature-based review. *J. Oral Biol. Craniofacial Res.* **2019**, *9*, 179–185. [[CrossRef](#)] [[PubMed](#)]
20. Etemad-Shahidi, Y.; Qallandar, O.B.; Evenden, J.; Alifui-Segbaya, F.; Ahmed, K.E. Accuracy of 3-Dimensionally Printed Full-Arch Dental Models: A Systematic Review. *J. Clin. Med.* **2020**, *9*, 3357. [[CrossRef](#)]
21. Shim, J.S.; Kim, J.E.; Jeong, S.H.; Choi, Y.J.; Ryu, J.J. Printing accuracy, mechanical properties, surface characteristics, and microbial adhesion of 3D-printed resins with various printing orientations. *J. Prosthet. Dent.* **2020**, *124*, 468–475. [[CrossRef](#)]
22. Unkovskiy, A.; Schmidt, F.; Beuer, F.; Li, P.; Spintzyk, S.; Kraemer Fernandez, P. Stereolithography vs. Direct Light Processing for Rapid Manufacturing of Complete Denture Bases: An In Vitro Accuracy Analysis. *J. Clin. Med.* **2021**, *10*, 1070. [[CrossRef](#)] [[PubMed](#)]
23. Hada, T.; Kanazawa, M.; Iwaki, M.; Arakida, T.; Soeda, Y.; Katheng, A.; Otake, R.; Minakuchi, S. Effect of Printing Direction on the Accuracy of 3D-Printed Dentures Using Stereolithography Technology. *Materials* **2020**, *13*, 3405. [[CrossRef](#)] [[PubMed](#)]
24. Palza, H. Antimicrobial polymers with metal nanoparticles. *Int. J. Mol. Sci.* **2015**, *16*, 2099–2116. [[CrossRef](#)]
25. González-Henríquez, C.M.; Sarabia-Vallejos, M.A.; Rodríguez Hernandez, J. Antimicrobial Polymers for Additive Manufacturing. *Int. J. Mol. Sci.* **2019**, *20*, 1210. [[CrossRef](#)]
26. Lin, C.H.; Lin, Y.M.; Lai, Y.L.; Lee, S.Y. Mechanical properties, accuracy, and cytotoxicity of UV-polymerized 3D printing resins composed of Bis-EMA, UDMA, and TEGDMA. *J. Prosthet. Dent.* **2020**, *123*, 349–354. [[CrossRef](#)] [[PubMed](#)]
27. Sultan, S.; Siqueira, G.; Zimmermann, T.; Mathew, A.P. 3D printing of nano-cellulosic biomaterials for medical applications. *Curr. Opin. Biomed. Eng.* **2017**, *2*, 29–34. [[CrossRef](#)]
28. Van Hengel, I.A.J.; Tierolf, M.; Valerio, V.P.M.; Minneboo, M.; Fluit, A.C.; Fratila-Apachitei, L.E.; Apachitei, I.; Zadpoor, A.A. Self-defending additively manufactured bone implants bearing silver and copper nanoparticles. *J. Mater. Chem. B* **2020**, *8*, 1589–1602. [[CrossRef](#)]
29. Yue, J.; Zhao, P.; Gerasimov, J.Y.; van de Lagemaat, M.; Grotenhuis, A.; Rustema-Abbing, M.; van der Mei, H.C.; Busscher, H.J.; Herrmann, A.; Ren, Y. 3D-Printable Antimicrobial Composite Resins. *Adv. Funct. Mater.* **2015**, *25*, 6756–6767. [[CrossRef](#)]
30. Garcia, C.; Gallardo, A.; López, D.; Elvira, C.; Azzahti, A.; Lopez-Martinez, E.; Cortajarena, A.L.; González-Henríquez, C.M.; Sarabia-Vallejos, M.A.; Rodríguez-Hernández, J. Smart pH-Responsive Antimicrobial Hydrogel Scaffolds Prepared by Additive Manufacturing. *ACS Appl. Bio Mater.* **2018**, *1*, 1337–1347. [[CrossRef](#)]
31. Haj Bloukh, S.; Edis, Z.; Abu Sara, H.; Alhamaidah, M.A. Antimicrobial Properties of Lepidium sativum L. Facilitated Silver Nanoparticles. *Pharmaceutics* **2021**, *13*, 1352. [[CrossRef](#)]
32. Syukri, D.M.; Nwabor, O.F.; Singh, S.; Ontong, J.C.; Wunnoo, S.; Paosen, S.; Munah, S.; Voravuthikunchai, S.P. Antibacterial-coated silk surgical sutures by ex situ deposition of silver nanoparticles synthesized with Eucalyptus camaldulensis eradicates infections. *J. Microbiol. Methods* **2020**, *174*, 105955. [[CrossRef](#)]
33. Choi, S.H.; Jang, Y.S.; Jang, J.H.; Bae, T.S.; Lee, S.J.; Lee, M.H. Enhanced antibacterial activity of titanium by surface modification with polydopamine and silver for dental implant application. *J. Appl. Biomater. Funct. Mater.* **2019**, *17*, 2280800019847067. [[CrossRef](#)] [[PubMed](#)]

34. Trindade, L.A.; de Araújo Oliveira, J.; de Castro, R.D.; de Oliveira Lima, E. Inhibition of adherence of *C. albicans* to dental implants and cover screws by *Cymbopogon nardus* essential oil and citronellal. *Clin. Oral Investig.* **2015**, *19*, 2223–2231. [[CrossRef](#)]
35. Ferrando-Magraner, E.; Bellot-Arcís, C.; Paredes-Gallardo, V.; Almerich-Silla, J.M.; García-Sanz, V.; Fernández-Alonso, M.; Montiel-Company, J.M. Antibacterial Properties of Nanoparticles in Dental Restorative Materials. A Systematic Review and Meta-Analysis. *Medicine* **2020**, *56*, 55. [[CrossRef](#)] [[PubMed](#)]
36. AlMojel, N.; AbdulAzees, P.A.; Lamb, E.M.; Amaechi, B.T. Determining growth inhibition of *Candida albicans* biofilm on denture materials after application of an organoselenium-containing dental sealant. *J. Prosthet. Dent.* **2021**, in press. [[CrossRef](#)]
37. Edis, Z.; Haj Bloukh, S.; Ibrahim, M.R.; Abu Sara, H. “Smart” Antimicrobial Nanocomplexes with Potential to Decrease Surgical Site Infections (SSI). *Pharmaceutics* **2020**, *12*, 361.
38. Santos, D.M.; Nagay, B.E.; da Silva, E.V.; Bonatto Lda, R.; Sonego, M.V.; Moreno, A.; Rangel, E.C.; da Cruz, N.C.; Goiato, M.C. In vitro analysis of different properties of acrylic resins for ocular prosthesis submitted to accelerated aging with or without photopolymerized glaze. *Mater. Sci. Eng. C Mater. Biol. Appl.* **2016**, *69*, 995–1003. [[CrossRef](#)] [[PubMed](#)]
39. Yagi, N.; Mori, M.; Hamamoto, A.; Nakano, M.; Akutagawa, M.; Tachibana, S.; Takahashi, A.; Ikehara, T.; Kinouchi, Y. Sterilization using 365 nm UV-LED. In Proceedings of the 2007 29th Annual International Conference of the IEEE Engineering in Medicine and Biology Society, Lyon, France, 22–26 August 2007; pp. 5842–5845. [[CrossRef](#)]
40. Peeters, E.; Nelis, H.J.; Coenye, T. Comparison of multiple methods for quantification of microbial biofilms grown in microtiter plates. *J. Microbiol. Methods* **2008**, *72*, 157–165. [[CrossRef](#)]
41. Choi, N.Y.; Kang, S.Y.; Kim, K.J. *Artemisia princeps* Inhibits Biofilm Formation and Virulence-Factor Expression of Antibiotic-Resistant Bacteria. *BioMed Res. Int.* **2015**, *2015*, 239519. [[CrossRef](#)]
42. M27-43. *Reference Method for Broth Dilution Antifungal Susceptibility Testing of Yeasts M27-A3*, 3rd ed.; Clinical and Laboratory Standards Institute: Wayne, PA, USA, 2008.
43. M 07-A9. *Methods for Dilution Antimicrobial Susceptibility Tests for Bacteria That Grow Aerobically: M07-A9*, 9th ed.; Clinical and Laboratory Standards Institute: Wayne, PA, USA, 2012.
44. Udroui, R.; Braga, I.C.; Nedelcu, A. Evaluating the Quality Surface Performance of Additive Manufacturing Systems: Methodology and a Material Jetting Case Study. *Materials* **2019**, *12*, 995. [[CrossRef](#)]
45. Arnold, C.; Monsees, D.; Hey, J.; Schweyen, R. Surface Quality of 3D-Printed Models as a Function of Various Printing Parameters. *Materials* **2019**, *12*, 1970. [[CrossRef](#)] [[PubMed](#)]
46. Revilla-León, M.; Jordan, D.; Methani, M.M.; Piedra-Cascón, W.; Özcan, M.; Zandinejad, A. Influence of printing angulation on the surface roughness of additive manufactured clear silicone indices: An in vitro study. *J. Prosthet. Dent.* **2021**, *125*, 462–468. [[CrossRef](#)]
47. Revilla-León, M.; Al-Haj Husain, N.; Methani, M.M.; Özcan, M. Chemical composition, surface roughness, and ceramic bond strength of additively manufactured cobalt-chromium dental alloys. *J. Prosthet. Dent.* **2021**, *125*, 825–831. [[CrossRef](#)]
48. Aravind Shanmugasundaram, S.; Razmi, J.; Mian, M.J.; Ladani, L. Mechanical Anisotropy and Surface Roughness in Additively Manufactured Parts Fabricated by Stereolithography (SLA) Using Statistical Analysis. *Materials* **2020**, *13*, 2496. [[CrossRef](#)] [[PubMed](#)]
49. Al-Qahtani, A.S.; Tulbah, H.I.; Binhasan, M.; Abbasi, M.S.; Ahmed, N.; Shabib, S.; Farooq, I.; Aldahian, N.; Nisar, S.S.; Tanveer, S.A.; et al. Surface Properties of Polymer Resins Fabricated with Subtractive and Additive Manufacturing Techniques. *Polymers* **2021**, *13*, 77. [[CrossRef](#)]
50. Pérez, M.; Medina-Sánchez, G.; García-Collado, A.; Gupta, M.; Carou, D. Surface Quality Enhancement of Fused Deposition Modeling (FDM) Printed Samples Based on the Selection of Critical Printing Parameters. *Materials* **2018**, *11*, 1382. [[CrossRef](#)] [[PubMed](#)]
51. Bollen, C.M.; Lambrechts, P.; Quirynen, M. Comparison of surface roughness of oral hard materials to the threshold surface roughness for bacterial plaque retention: A review of the literature. *Dent. Mater. Off. Publ. Acad. Dent. Mater.* **1997**, *13*, 258–269. [[CrossRef](#)]
52. Teughels, W.; Van Assche, N.; Sliepen, I.; Quirynen, M. Effect of material characteristics and/or surface topography on biofilm development. *Clin. Oral Implant. Res.* **2006**, *17*, 68–81. [[CrossRef](#)] [[PubMed](#)]
53. Anselme, K.; Davidson, P.; Popa, A.M.; Giazzon, M.; Liley, M.; Ploux, L. The interaction of cells and bacteria with surfaces structured at the nanometre scale. *Acta Biomater.* **2010**, *6*, 3824–3846. [[CrossRef](#)] [[PubMed](#)]
54. Scheuerman, T.R.; Camper, A.K.; Hamilton, M.A. Effects of Substratum Topography on Bacterial Adhesion. *J. Colloid Interface Sci.* **1998**, *208*, 23–33. [[CrossRef](#)] [[PubMed](#)]
55. Engel, A.S.; Kranz, H.T.; Schneider, M.; Tietze, J.P.; Piwowarczyk, A.; Kuzius, T.; Arnold, W.; Naumova, E.A. Biofilm formation on different dental restorative materials in the oral cavity. *BMC Oral Health* **2020**, *20*, 162. [[CrossRef](#)]
56. Ahimou, F.; Denis, F.A.; Touhami, A.; Dufréne, Y.F.J.L. Probing microbial cell surface charges by atomic force microscopy. *Langmuir* **2002**, *18*, 9937–9941. [[CrossRef](#)]
57. Steiner, H.; Hultmark, D.; Engström, A.; Bennich, H.; Boman, H.G. Sequence and specificity of two antibacterial proteins involved in insect immunity. *Nature* **1981**, *292*, 246–248. [[CrossRef](#)]
58. Kozmos, M.; Virant, P.; Rojko, F.; Abram, A.; Rudolf, R.; Raspor, P.; Zore, A.; Bohinc, K. Bacterial Adhesion of *Streptococcus mutans* to Dental Material Surfaces. *Molecules* **2021**, *26*, 1152. [[CrossRef](#)]

59. Du, Y.; Xu, J.; Sakizadeh, J.D.; Weiblen, D.G.; McCormick, A.V.; Francis, L.F. Modulus- and Surface-Energy-Tunable Thiol-ene for UV Micromolding of Coatings. *ACS Appl. Mater. Interfaces* **2017**, *9*, 24976–24986. [[CrossRef](#)] [[PubMed](#)]
60. Park, S.E.; Periathamby, A.R.; Loza, J.C. Effect of surface-charged poly(methyl methacrylate) on the adhesion of *Candida albicans*. *J. Prosthodont Off. J. Am. Coll. Prosthodont.* **2003**, *12*, 249–254. [[CrossRef](#)]
61. Yang, N.; Zhang, D.D.; Li, X.D.; Lu, Y.Y.; Qiu, X.H.; Zhang, J.S.; Kong, J. Topography, Wettability, and Electrostatic Charge Consist Major Surface Properties of Intraocular Lenses. *Curr. Eye Res.* **2017**, *42*, 201–210. [[CrossRef](#)] [[PubMed](#)]
62. Minagi, S.; Miyake, Y.; Inagaki, K.; Tsuru, H.; Suginaka, H. Hydrophobic interaction in *Candida albicans* and *Candida tropicalis* adherence to various denture base resin materials. *Infect. Immun.* **1985**, *47*, 11–14. [[CrossRef](#)]
63. Klotz, S.A.; Drutz, D.J.; Zajic, J.E. Factors governing adherence of *Candida* species to plastic surfaces. *Infect. Immun.* **1985**, *50*, 97–101. [[CrossRef](#)] [[PubMed](#)]
64. Collier, T.O.; Jenney, C.R.; DeFife, K.M.; Anderson, J.M. Protein adsorption on chemically modified surfaces. *Biomed. Sci. Instrum.* **1997**, *33*, 178–183.
65. Klotz, S.A. The contribution of electrostatic forces to the process of adherence of *Candida albicans* yeast cells to substrates. *FEMS Microbiol. Lett.* **1994**, *120*, 257–262. [[CrossRef](#)]
66. Turner, R.D.; Wingham, J.R.; Paterson, T.E.; Shepherd, J.; Majewski, C. Use of silver-based additives for the development of antibacterial functionality in Laser Sintered polyamide 12 parts. *Sci. Rep.* **2020**, *10*, 892. [[CrossRef](#)] [[PubMed](#)]
67. Van Hengel, I.A.J.; Putra, N.E.; Tierolf, M.; Minneboo, M.; Fluit, A.C.; Fratila-Apachitei, L.E.; Apachitei, I.; Zadpoor, A.A. Biofunctionalization of selective laser melted porous titanium using silver and zinc nanoparticles to prevent infections by antibiotic-resistant bacteria. *Acta Biomater.* **2020**, *107*, 325–337. [[CrossRef](#)]
68. Van Hengel, I.A.J.; Riool, M.; Fratila-Apachitei, L.E.; Witte-Bouma, J.; Farrell, E.; Zadpoor, A.A.; Zaat, S.A.J.; Apachitei, I. Selective laser melting porous metallic implants with immobilized silver nanoparticles kill and prevent biofilm formation by methicillin-resistant *Staphylococcus aureus*. *Biomaterials* **2017**, *140*, 1–15. [[CrossRef](#)] [[PubMed](#)]
69. El Moussaoui, A.; Jawhari, F.Z.; Almehdi, A.M.; Elmsellem, H.; Fikri Benbrahim, K.; Bousta, D.; Bari, A. Antibacterial, antifungal and antioxidant activity of total polyphenols of *Withania frutescens*. *Bioorganic Chem.* **2019**, *93*, 103337. [[CrossRef](#)] [[PubMed](#)]
70. Dantas, K.N.M.; Andrade, L.R.; Lisboa, E.; Santana, V.L.; Santos, A.L.S.; Mello, T.P.; Sengenito, L.S.; Lima, Á.S.; Fricks, A.T.; Begnami, A.F.; et al. Antimycotic nail polish based on humic acid-coated silver nanoparticles for onychomycosis. *J. Chem. Technol. Biotechnol.* **2021**, *96*, 2208–2218. [[CrossRef](#)]